Soft Matter

Accepted Manuscript

ROYAL SOCIETY OF CHEMISTRY

www.rsc.org/softmatter

Journal Name

ARTICLE TYPE

Cite this: DOI: 10.1039/xxxxxxxxxx

Mesh size analysis of cellulose nanofibril hydrogels with solute exclusion and PFG-NMR spectroscopy

Leila Jowkarderis,[a] Theo G. M. van de Ven*[b]

Received Date
Accepted Date

DOI: 10.1039/xxxxxxxxxx

www.rsc.org/journalname

The pore structure of TEMPO-mediated oxidized CNF hydrogels, chemically cross-linked with water-soluble diamines, is studied. Solute exclusion method and pulsed-field-gradient NMR are used to estimate the mesh size distribution in the gel network in its hydrated state. Dextran fractions with the nominal molecular wights in the range 10-2000 kDa are used as probes. The results show a nonuniform network structure, consisting of a group of large openings that contain $\sim 50\%$ of the water, and regions with a more compact structure and smaller mesh units that restrict the diffusivity of the dextran molecules. A biexponential model is proposed for the NMR echo amplitude decay due to the probe diffusion into the gel network. Typical single exponential model does not fit the experimental data when the probe molecular size is comparable to the network mesh size. The results obtained with NMR, using the proposed biexponential model, are in very good agreement with those determined with solute exclusion. Precise mesh size estimation with solute exclusion using pore models is subject to restrictions, and vary with the assumed pore geometry. The average mesh size obtained using spherical pore model, ~ 35 nm, in the compact regions of the hydrogel, is in good agreement with the theoretical value in a network of rodlike particles. Neglecting the wall effects leads to underestimation of the mesh size with both techniques.

1 Introduction

Cellulose nanofibrils (CNF) are the smallest components of wood, with a diameter of about 4 nm, and a length of a few microns.[1] The large surface area and high aspect ratio of nanofibrils, along with the fact that cellulose is a biodegradable natural polymer, have attracted significant interest to use CNF in various applications. CNF has been suggested as rheology modifier in food, paint, and cosmetics,[2] as filler in nanocomposites,[3] as barrier in food packaging,[4] and more recently, as a promising biomedical material.[5–8]

Decomposition of wood fibres into cellulose nanofibrils is carried out with chemical pretreatments, such as enzymatic hydrolysis, carboxymethylation, quaternization, and TEMPO-mediated oxidation of wood pulp, followed by mechanical treatments.[1,9–12] Chemical methods are mainly based on introducing negatively charged groups onto the surface of nanofibrils, and inducing electrostatic repulsions between them, which facilitates the mechanical disintegration in the following step. Cellulose nanofibrils in water make three-dimensional networks and viscous suspensions with high mechanical strength. We have studied the viscoelastic properties of these suspensions in the dilute and semi-dilute regimes previously.[13,14]

Chemical cross-linking of nanofibrils through the surface charged functional groups increases the stiffness of CNF suspensions. Cross-linked nanocellulose based hydrogels have been recently studied for biomedical applications such as drug delivery.[5,7,15,16] Using CNF hydrogels for biomedical purposes necessitates a detailed study of their microstructure and porosity. Drug delivery applications involve diffusion of drug molecules through the hydrogel network, which is controlled mainly by the network mesh size. The mesh size may depend on the fibril dimensions, fibril consistency, the cross-linking agent, and the degree of cross-linking. Masruchin et. al. (2015) studied TEMPO-oxidized CNF hydrogels, focusing on their drug-release properties.[17] Cross-linking was induced using cations Al^{3+}, Ca^{2+} and H^{+}. They freeze-dried the hydrogels to investigate their internal morphology and pore size with field emission scanning electron microscopy (FE-SEM), and with the Barrett-Joyner-Halenda (BJH) method, which is based on the amount of nitrogen desorption from the pores of the material. They did not observe any significant difference in the morphology and the pore diameter of the hydrogels prepared using Al^{3+} or Ca^{2+}, while the protonated hydrogel contained larger openings.

[a] Department of Chemical Engineering, McGill University, Montreal, Quebec H3A 0C5
[b] Pulp & Paper Research Center and Department of Chemistry, McGill University, Montreal, Quebec H3A 2A7 Fax: +1 (514)398-8254; Tel: +1 (514)398-6177; E-mail: theo.vandeven@mcgill.ca

There are other techniques that can be used for pore size distribution analysis, such as transmission electron microscopy (TEM) and mercury intrusion porosimetry. These methods, however, are usually restricted to dry samples. Removing water from the hydrogel may change its network structure and mesh size. Also, in biomedical applications, hydrogels are used in their native hydrated state. Therefore, techniques that can measure the network mesh size in the wet state are required.

Solute exclusion or inverse size-exclusion chromatography has been used to study the mesh structure of polymeric networks.[18–21] Solute exclusion was introduced by Aggerbrandt and Samuelson (1964) to study the penetration of polymer molecules into the cellulose fibres.[22] The method was then employed to measure the pore structure of wet fibre wall using macromolecules that do not adsorb onto the fibres, such as dextran or polyethylene glycol.[23–26] A solute molecule with a certain size does not diffuse into a pore that is smaller than its molecular size. Therefore, using a set of macromolecules with various sizes, one can estimate the pore size distribution in the fibre wall or in a fibrous network. This method can be used to study CNF hydrogels in the hydrated state.

The pore size can be also estimated from the ratio of the diffusion coefficient of the probe molecules in the gel network, to their diffusion coefficient in the solvent.[27,28] The diffusivity of the probe molecules in the aqueous medium can be measured with pulsed-field-gradient NMR (PFG-NMR).[29,30] Wallace et. al. (2013) studied the mesh structure of naphthalene diphenylalanine hydrgels, prepared with the addition of Ca^{2+}, using PFG-NMR.[29] They measured the diffusivity of dextran molecules with nominal molecular weights ranging from 6 to 2000 kDa, in the absence and presence of a network, and estimated an average mesh size in their sample. However, they could not obtain precise diffusion coefficients for the large dextran fractions, 1400 and 2000 kDa, in the gel phase. They attributed this to the trapping of the large dextran molecules by the gel network.

In this paper, TEMPO-mediated oxidized CNF suspensions are cross-linked using water-soluble diamines, such as diaminooctane (DAO), diaminobutane (DAB), and adipic acid dihydrazide (ADH). Mesh size analysis is carried out with solute exclusion, and with PFG-NMR, using dextran fractions with molecular weights in the range 10-2000 kDa as probe molecules. All the computations are done with MATLAB.

2 Methods

2.1 Pore size estimation with solute exclusion

Solute exclusion estimates the pore size distribution based on the accessibility of the pores to macromolecules that do not adsorb onto the pore wall. When a probe molecule is larger than a pore, it gets excluded from that pore. This is the opposite of size-exclusion chromatography (SEC), which is used to measure the size distribution of an unknown solute. When the solute molecular size is known, SEC can characterize the porous medium, therefore the technique is called inverse size-exclusion chromatography. Here we apply this method, using a set of dextran fractions as probe molecules, to study CNF hydrogels. The procedure is as follows. When a CNF hydrogel, with a defined mass of water w_w and a defined mass of fibril w_f, is exposed to a known amount of a dextran solution w_s with a defined initial concentration c_i, a portion of the total water in the gel is accessible to the dextran molecules, and the rest of the water q is inaccessible. Dextran molecules diffuse into the hydrogel pores, therefore, the dextran concentration in the solution phase decreases with time until reaching equilibrium. The final concentration will be then c_f in w_s+w_w-q amount of solution. From the fact that the total amount of dextran has not changed, the amount of inaccessible water can be estimated by[23,25,26]

$$\sigma = \frac{q}{w_f} = \frac{(w_s + w_w)}{w_f}[1 - \frac{w_s}{w_s + w_w}\frac{c_i}{c_f}]. \quad (1)$$

The amount of inaccessible water per gram fibril, σ, increases with increasing the probe size, reaching a plateau $\sigma_{plateau}$ at large molecular sizes, when the probes cannot diffuse into any of the pores. In case of a water-swollen fibre wall, this plateau shows the total amount of water associated with all the pores in the fibre wall, called the fibre saturation point σ = FSP.[26] For saturated hydrogels, the upper limit of σ is equal to the swelling capacity of the hydrogel.[21] If all the pores in a network are larger than a minimum size, a plateau equal to zero is also observed at small molecular sizes, meaning that the macromolecules that are smaller than a certain size, have access to all the pores in the network.

It has been suggested that the derivative of the best mathematical fit to the σ values as a function of probe hydrodynamic radius R_h, gives an estimation of the pore size distribution. Since the characteristic shape of the $\sigma(R_h)$ curve is S-shaped, a logistic function with equation

$$y(x) = \frac{\alpha}{1 + e^{(\beta - \gamma x)}} \quad (2)$$

is used to fit the $\sigma(R_h)$ data, where α, β and γ are fitting parameters, x corresponds to R_h, and $y(x)$ corresponds to the σ values.[20,23,25,31] In this approach, it is assumed that when a pore is larger than a solute molecule, all the water in the pore is accessible to that molecule. However, in reality, the macromolecule cannot move in the entire volume inside the pore with equal probability, due to the wall effects. Therefore, approximating the pore size distribution directly from the cumulative $\sigma(R_h)$ curve my lead to underestimation of the mesh size.

The concentration of a non-adsorbing molecule is zero on the surface of the pore wall. A layer adjacent to the pore wall, over which the concentration changes from zero on the wall to the bulk value at a distance from the wall, is called the depletion layer. The depletion layer affects the partitioning of the solute molecules between the gel and the solution phase, since the solute molecules have limited access to the water in this layer. The depletion layer thickness typically scales with the particle size R_h. Therefore, the local partition coefficient K, here defined as the fraction of water accessible to a molecule in a pore with radius r, depends on the molecule size, and the pore geometry, when the molecule is smaller than the pore $R_h < r$. If $R_h > r$, $K = 0$, meaning that the solute molecules are completely excluded from the pore. Consid-

ering the wall effects, Casassa (1967) developed expressions for $K(R_h, r)$ for simple pore geometries such as slit-like, cylindrical, and spherical pores, as follows:[32,33]

$$K_{slit} = \frac{8}{\pi^2}\Sigma_{n=0}^{\infty}\frac{1}{(2n+1)^2}\exp[-\frac{(2n+1)^2\pi^2}{4}(\frac{R_h}{r})^2], \quad (3)$$

$$K_{cylinder} = 4\Sigma_{n=1}^{\infty}\frac{1}{\beta_n^2}\exp[-\beta_n^2(\frac{R_h}{r})^2], \quad (4)$$

$$K_{sphere} = \frac{6}{\pi^2}\Sigma_{n=1}^{\infty}\frac{1}{n^2}\exp[-n^2\pi^2(\frac{R_h}{r})^2], \quad (5)$$

where β_n is the nth zero of the Bessel function $J_0(\beta)$. The total amount of water accessible to a molecule with radius R_h in the whole gel phase is then

$$1 - \frac{\sigma}{\sigma_{plateau}} = \int_0^{\infty} K(R_h, r)f(r)dr, \quad (6)$$

where $f(r)$ is the normalized pore size distribution i.e., $\int_0^{\infty} f(r)dr = 1$. Assuming all the pores have the same radius r, equation 6 reduces to

$$\frac{\sigma}{\sigma_{plateau}} = 1 - K(R_h, r). \quad (7)$$

An average pore size r can be then estimated with fitting the $\sigma(R_h)$ data to equation 7. However, there are uncertainties associated with using this model for gels. A slit-like pore model is reasonable in the cell wall,[26] due to its lamellar structure. But in a gel network, the openings between the fibrils have complex structures and are not expected to be simple slits, or cylinders, or spheres. It has been recently shown that a simple-geometry pore model does not successfully predict the partition coefficient of the cross-linked polymer gels, and overestimates the mesh size, when dilute solutions of probe molecules are used.[34] On the other hand, it has been suggested that solute exclusion, in general, may underestimate the pore size. Because the osmotic pressure difference between the pore interior and the bulk solution may cause the pore contraction, and in case of hydrogels, it may make the gel deswell.[21,35–37] Despite the mentioned issues, solute exclusion is still considered as a valuable technique for the determination of the "effective pore size" and the "effective accessible water",[33,35] and the simple-geometry pore models have been widely used for a rough estimation of the pore size in fibrous and polymeric networks.[18,19,21,38]

In this paper we analyse the solute exclusion data using the logistic function, and the three introduced pore models, and compare the results with those obtained using NMR, and those predicted by theory.

2.2 Pore size estimation based on probe diffusivity

When a dextran molecule with hydrodynamic radius R_h diffuses into a network with an average mesh size ξ, its diffusivity is restricted by the network. The diffusion coefficient of the probe molecule in the network D is related to the mesh size by[28,29]

$$\frac{D}{D_0} = \exp[-\frac{R_h}{\xi}]^{\delta}, \quad (8)$$

where D_0 is the diffusion coefficient in a dilute solution, and $\delta \approx 1$, is a system-dependent parameter.[29] This equation was derived based on the decrease in the entropy of a mesh unit when it expands to the size R_h, neglecting the finite width of the fibrils forming the network. Similar equations can be obtained based on the hydrodynamics of polymer solutions.[39,40] Equation 8 has been shown to give good fits to the diffusivity data in various systems, as well as reasonable estimates of the mesh size.[29,40] Amsden (1999) on the other hand, considered the finite radius of the fibrils, suggesting[41]

$$\frac{D}{D_0} = \exp[-\frac{\pi}{4}(\frac{R_f + R_h}{R_f + R_p})^2], \quad (9)$$

where R_p is the average pore radius, in a fibril network with fibril radius R_f.

2.3 Diffusion coefficients determination with PFG-NMR

The diffusion coefficient D of molecules in solution can be measured with pulsed-field-gradient NMR, based on the exponential attenuation of the NMR echo amplitude due to translational diffusion. Assuming a Gaussian distribution for the displacements due to diffusion, the amplitude intensity of the PFG-NMR signal is related to D by[30,42]

$$\frac{A(2\tau)}{A_0} = \exp[-(\gamma\delta G)^2(\Delta - \delta/3)D]. \quad (10)$$

In this equation, $A(2\tau)$ and A_0 are the echo amplitudes at t $= 2\tau$ with and without the magnetic field gradient, respectively, where 2τ is the time at which, the signal attenuates due to diffusion, γ is the ^{1}H gyromagnetic ratio with the value $\gamma/2\pi = 4257.6$ s^{-1}Gauss^{-1}, δ is the pulsed field gradient duration (s), which should not be mistaken with the δ in equation 8, G is the gradient strength (Gauss m^{-1}), and Δ is the time between the gradient pulses (s). For poly dispersed samples, a stretched exponential expression is suggested as[43]

$$\frac{I}{I_0} = \exp(-bD')^{\beta}, \quad (11)$$

where I and I_0 are signal intensities with and without the magnetic field gradient, D' is a fitting parameter, β is the stretching exponent, and $b = (\gamma\delta G)^2(\Delta - \delta/3)$. The mean inverse diffusion coefficient can be then estimated by

$$\langle\frac{1}{D}\rangle = \frac{1}{\beta D'}\Gamma(\frac{1}{\beta}), \quad (12)$$

where Γ is the gamma function.

2.4 Determination of R_h

The hydrodynamic radius R_h of a probe molecule can be experimentally measured with dynamic light scattering DLS. When the diffusion coefficient D_0 of the macromolecule in the dilute solution is measured with NMR, R_h can be obtained with Stokes-Einstein equation

$$R_h = \frac{K_B T}{6\pi\eta D_0}, \quad (13)$$

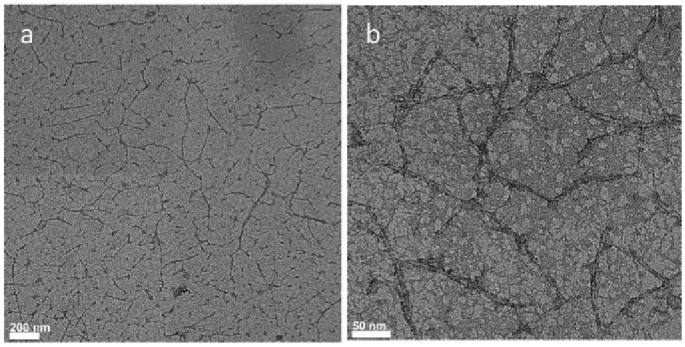

Fig. 1 TEM micrographs of cellulose nanofibrils. a) The scale bar corresponds to 200 nm. b) The scale bar corresponds to 50 nm.

where K_B is the Boltzmann constant, T is the absolute temperature, and η is the viscosity of the solvent. As another option, R_h (nm) is theoretically related to the molecular weight M_w (Da) as[44]

$$R_h = 0.015 M_w^{0.53 \pm 0.02}. \quad (14)$$

3 Experimental

3.1 CNF sample

A 0.9% w/w carboxylated CNF suspension, prepared with TEMPO-mediated oxidation using NaClO, was received from the Forest Product Laboratory FPL (Madison, WI). The manufacturer reported a carboxyl density of 1.2 mmol g^{-1} dry CNF, in the form COONa. In this work, all the measurements were done at neutral pH, and 0.7% w/w CNF consistency, diluting the original sample with deionized water.

The CNF sample was characterized with transmission electron microscopy (TEM), using a Tecnai T-12 instrument, operating at 120 kV. A copper grid was first coated with a 0.01 M poly-L-lysine solution. A 0.001% w/w CNF suspension was then deposited onto the grid, and was allowed to dry. The sample was stained using a 0.2% w/w uranyl acetate solution. Figure 1 shows the TEM micrographs of the CNF sample at two different magnifications. An average width of ~ 4 nm, and an average length of ~ 600 nm are estimated for this sample.

3.2 Chemical cross-linking

The CNF suspensions were chemically cross-linked through the surface carboxyl groups. 1-4 diaminobutane (DAB), 1-8 diaminooctane (DAO), and adipic acid dihydrazide (ADH) were used as cross-linkers. 4-(4,6- dimethoxy-1,3,5-triazin-2-yl)-4-methylmorpholinium chloride (DMT-MM) was used as the reaction activator.[45] All the diamines and the activator were purchased from Sigma-Aldrich.

A standard 1 M solution of each cross-linker in deionized water was prepared. The 0.7% w/w CNF suspensions were prepared with adding the 0.9% w/w suspension to the solutions containing the corresponding amount of DMT-MM, for a ratio of 1 mol DMT-MM mol^{-1} COO^-, in deionized water. The samples were stirred for 2 min to ensure uniform dispersion. Diamine solutions were then added to the suspensions with a micropipet, to make a ratio of 0.5 mol diamine mol^{-1} COO^-. The samples were stirred for 1 min. The reactions were then allowed to complete over night without stirring, to avoid network breakage. The liquid-like 0.7% w/w CNF suspensions were converted into self-holding gels, due to inter and intra fibrillar cross-linking. The interfibrillar cross-linking at the fibril-fibril contact points strengthens the network structure. The interfibrillar cross-linking at the amorphous regions of the nanofibrils stiffens the rods and increases their rigidity, causing an increase in the mechanical strength of the cross-linked gel. The whole procedure was done at room temperature.

3.3 Solute exclusion experiment

Cross-linked 0.7% w/w CNF suspensions were prepared in glass vials, in three sets, using one of the diamines, DAB, DAO, and ADH. Dextran fractions, with nominal molecular weights 10, 40, 70, 110, 500 and 2000 kDa, were purchased from Pharmecia, Sweden. Two grams of 5% w/w dextran solutions were prepared and added to the vials containing two grams of CNF hydrogel. The vials (Fisherbrand, 28 mm diameter) were sealed to prevent water evaporation. The process was then stopped after one day, with the removal of the dextran solutions. Pre-experiments were done to find the time required to reach equilibrium in dextran concentration. Similar results were obtained after one, two, and three days, suggesting that equilibrium is reached before one day (data available in the ESI, figure 1). The final dextran concentration was determined with evaporating a known amount of the solution in an oven at 105°C for four hours. The whole process was carried out in duplicate, including the hydrogel preparation step. All the tests were done at room temperature.

Swelling potential of the hydrogels, with respect to the initial volume of the cross-linked 0.7% w/w hydrogel, was determined in deionized water, and in 5% w/w solutions of dextrans 70 and 110 kDa. The cross-linked 0.7% w/w CNF hydrogels were exposed to water or dextran solutions in sealed vials for one week. A 20% swelling was observed in the hydrogel that was in contact with deionized water. No swelling or deswelling was observed in the hydrogels that were exposed to dextran solutions. This indicates that the osmotic pressure difference between the solution and the gel phase in our system prevents gel swelling, but it is not large enough to collapse the gel. Under such experimental conditions, we can safely assume that the fibril network is stable, and the mesh units do not expand or contract during our measurements.

Returning to equation 1, in this system, $w_s = 2$ g, $c_i = 5\%$ w/w, and $w_w = 1.986$ g, and $w_f = 0.014$ g. If the dextran molecules are large enough not to diffuse into the hydrogel pores at all, we expect the plateau to be equal to the total amount of water used to make the hydrogel per gram fibril, w_w/w_f, which we consider as σ_{max}.

The final dextran concentration c_f, measured with evaporation, varied in the range 2.6-3.5% w/w, depending on the size of the dextran molecules in the solution. It must be mentioned that the amount of diamine and the reaction activator used to prepare

the hydrogels is small. If the DMT-MM molecules or the non-reacted diamine molecules happen to diffuse from the gel phase into the solution during the experiments, their effect on the measurement of c_f is negligible.

3.4 NMR experiment

To measure the diffusivity of the dextran probes in the dilute solution, an aqueous solution, containing 20% w/w D_2O, of each dextran fraction was prepared with 0.1% w/w dextran consistency. The solutions were then transferred into 5 mm NMR tubes with a pipet.

To measure the diffusion coefficients in the CNF network, 0.7% CNF suspensions, each containing 20% w/w D_2O, 0.1% w/w of a dextran fraction, and the required amount of DMT-MM, were prepared. CNF suspensions were then cross-linked with the addition of DAO and stirring for 1 min. The suspensions were transferred into 5 mm NMR tubes right away, and the reaction was allowed to complete over night, inside the tubes. All the samples were tested the day after preparation.

The experiments were recorded on a 500 MHz Varian INOVA NMR spectrometer, using a 1H-13C-15N triple-resonance room temperature probe, equipped with z-axis pulsed field gradients. Peaks related to dextran in the dilute solutions and in the cross-linked hydrogels were clearly recognizable in the NMR spectra. The echo amplitude A was recorded as a function of the gradient strength G, using a water-suppressed LED pulse sequence,[42] with G changing in the range 1.9-46 Gauss cm^{-1}. Measurements were done with Δ varying in the range 0.25-1 s, and the gradient durations δ in the range 2.5-5 ms, depending on the dextran molecular size. The larger the probe molecule, the longer the time necessary to observe diffusion. All the tests were done at 25°C.

The signal intensity data were fitted to equation 10 with A_0 and D as free parameters, and to equation 11 with I_0, D', and β as free parameters.

3.5 DLS

Dextran solutions with 0.2% w/w consistency were prepared. Dust free samples were obtained with filtering the dextran solutions through 0.22 μm syringe filters. The average R_h for each fraction was measured using a Brookhaven light scattering instrument, with a polarized laser operating at $\lambda = 532$ nm. The scattered light intensity at 90 degrees was monitored for 10 minutes in each test. The temperature was set to 25 °C. Measurements were done in triplicate.

4 Results and discussion

4.1 Hydrodynamic radius

Hydrodynamic radius of each dextran fraction was estimated using equation 13, with diffusion coefficients D_0 and the viscosity of the solvent η as known parameters. Diffusion coefficients D_0 were measured fitting the PGF-NMR intensity data, obtained for each dextran fraction in an aqueous medium, to equations 10 and 11. Figure 2 shows the echo amplitude as a function of gradient strength square G^2 for dextran 500 kDa in aqueous medium, with a fit to equation 10, as an example. Similar results were acquired using both equations, as $\beta > 0.99$ was obtained in all cases. The corresponding R_h values were then calculated with equation 13. Table 1 shows the R_h obtained with the Stokes equation 13, considering $\eta \sim 0.9$ mPa s for the water/D_2O mixture, as well as the values calculated theoretically with equation 14, and the data acquired with DLS.

Table 1 Diffusion coefficients in the dilute aqueous solution D_0 (m^2 s^{-1}), obtained fitting equation 10 to the experimental data with the goodness of fit R^2, and the corresponding hydrodynamic radius R_h (nm) obtained with Stokes equation 13, calculated theoretically with equation 14, and measured with DLS, for all dextran fractions (kDa)

M_w	$D_0 \times 10^{11}$	R^2	$R_{h,Stokes}$	$R_{h,theory}$	$R_{h,DLS}$
10	10.7	0.99	2.3	2.0±0.4	2.3±1.5
40	5.5	0.99	4.4	4.2±0.9	4.8±1.2
70	4.3	0.99	5.7	5.6±1.3	6.0±2.6
110	3.4	0.99	7.1	7.2±1.7	7.6±2.7
500	1.9	0.99	13	16±4.2	14±9.0
2000	1.3	0.99	19	34±9.7	40±20

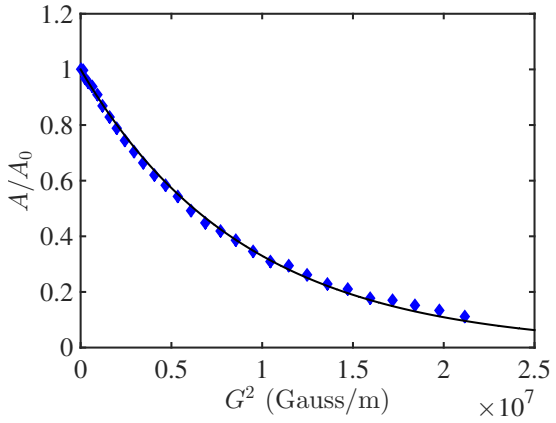

Fig. 2 Normalized echo amplitude vs. G^2 for dextran 500 kDa in water and 20% w/w D_2O, $\delta = 0.004$ s, $\Delta = 0.5045$ s. The line is a fit to equation 10.

Our results are in good agreement with the data reported by Wallace et. al. (2013).[29] Similar R_h values are obtained with NMR and with equation 14 for smaller dextrans, 10-110 kDa. For dextrans 500 and 2000 kDa, however, the measured $R_{h,Stokes}$ is smaller than the theoretical value. This could be due to the polydispersity of the dextran fractions, and thus the presence of many particles with smaller molecular weights than their nominal values.[29] The results obtained with DLS are in agreement with the $R_{h,Stokes}$ values for dextrans 10-500 kDa, but for dextran 2000 kDa, $R_{h,DLS} \sim 2R_{h,Stokes}$.

The mesh size analysis in this paper is carried out using the $R_{h,Stokes}$ values measured with PFG-NMR.

4.2 Solute exclusion

The amount of inaccessible water normalized with respect to the total amount of water in the hydrogel, σ/σ_{max}, is shown in figure 3, as a function of the probe hydrodynamic diameter d_h. The results obtained for CNF hydrogels prepared using DAO and DAB are almost similar, but the σ value obtained for the hydrogel prepared with ADH seems to be slightly smaller than the other

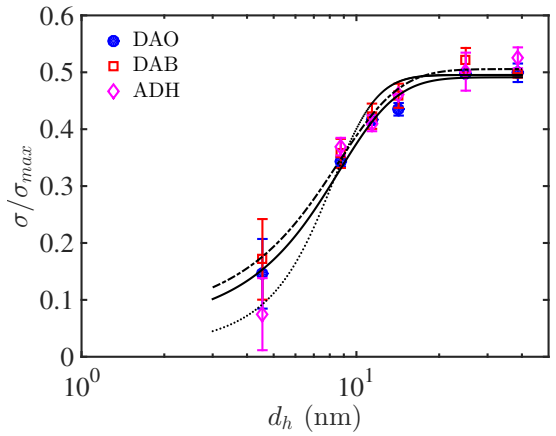

Fig. 3 σ/σ_{max} vs. d_h for 0.7% CNF hydrogels prepared with the three diamines. The lines are to guide the eye.

two samples at $d_h \sim 4.6$ nm. This indicates that the minimum pore size in this hydrogel is larger than the minimum pore size in the hydrogels prepared with DAO or DAB. This is consistent with our rheometry results, showing smaller elastic and viscous moduli for the hydrogel prepared with ADH, compared to those prepared with the other two diamines (data available in the ESI, figure 2), since the smaller the pore size, the higher the mechanical strength of the hydrogel, and therefore, the larger the elastic modulus.[29,46–48] The σ/σ_{max} ratio increases with increasing the probe molecular size, reaching a plateau at $d_h \sim 20$ nm, with a plateau value of $\sigma/\sigma_{max} \sim 0.5$.

The fact that the amount of inaccessible water at the plateau $\sigma_{plateau}$ is not equal to the total amount of water in the hydrogel can be explained by two causes. The first hypothesis is that the osmotic pressure difference between the CNF hydrogel and the dextran solution is large enough to transfer half of the water from the gel phase to the solution. Consequently, the hydrogel should collapse to half of its original volume. However, as mentioned previously, the cross-linked CNF hydrogels exposed to dextran solutions, do not swell or collapse during our measurements. Therefore, the osmotic forces cannot be the reason for $\sigma_{plateau}/\sigma_{max} \sim 0.5$. The second hypothesis is that even the largest dextran fractions used here, 500 and 2000 kDa, have access to almost half of the water (1-$\sigma_{plateau}/\sigma_{max}$) in the hydrogel. This suggests that there are two sets of mesh units in this network: one, a number of large pores, containing half of the water in the hydrogel structure, that are accessible to all the dextran fractions, and two, a group of smaller pores in regions with a more compact structure, containing the second half of the water, where the dextran molecules with $d_h \gtrsim 20$ nm do not have access to. This hypothesis is reasonable considering the heterogenous structure of CNF hydrogels. In addition, the cross-linking procedure increases the heterogeneity of the fibril network, because the nonuniform distribution of the cross-linking agents may induce compact regions with a high degree of cross-linking, and areas with large opening in the hydrogel structure.

To estimate the mesh size distribution, we fit the $\sigma(d_h)$ data obtained for the CNF hydrogels cross-linked with DAO, to the logistic function and the simple-geometry pore models introduced previously. As shown in figure 4a, equation 2 fits the experimental data very well, with α, β, and γ equal to 0.5, 2.8, and 0.4, respectively. The pore size distribution obtained from the derivative of this mathematical function shows an average pore diameter of ~ 7 nm, with a maximum diameter of ~ 20 nm. In this model, the derivative of $\sigma(d_h)$ curve matters and not the exact $\sigma(d_h)$ values. Thus, the obtained average and maximum pore diameter represent the set of smaller pores in the compact regions of the hydrogel. The $d_h \sim 20$ nm, at which the plateau begins, is automatically considered as the upper extreme of the pore size distribution, no matter how big the $\sigma(d_h)$ is. However, even considering only the dense parts of the hydrogel, the pore size is still underestimated with this model, due to neglecting the wall effects. The pore models suggest that the smallest pore that a dextran molecule can have access to should be twice as large as the dextran size, due to the presence of depletion layers, which can be as thick as the dextran size. Therefore, the maximum pore diameter in the compact regions can be as large as ~ 40 nm.

To obtain an average pore size using the simple-geometry pore models, we normalize the σ values, acquired for the same hydrogel, with respect to $\sigma_{plateau}$, not σ_{max}, to meet the upper boundary condition of these models. The complete exclusion of solute, or the inaccessibility of the total amount of water in the pores, corresponds to when $\sigma(d_h)$ curve reaches a plateau in the pore models. Normalizing σ values to $\sigma_{plateau}$ secures $K = 0$ at the plateau. The estimated pore size is thus only for the set of smaller pores in the compact regions of the gel network. Figure 4b illustrates the experimental $\sigma(d_h)$ data and fits to equation 7, with $K(R_h, r)$ for the three different pore geometries shown in equations 3 - 5. The predicted pore size is completely geometry dependent. An average pore diameter of 15 nm, assuming slit-like pores, 25 nm, for cylindrical pores, and 35 nm, assuming spherical pores, is obtained for the dense parts of this system. These values are noticeably larger than the one obtained with the best mathematical fit model, due to considering the wall effects.

4.3 Self diffusion

Diffusion coefficients of the dextran molecules in the CNF hydrogels prepared using DAO were estimated fitting the NMR intensity data to equations 10 and 11. Similar to the diffusivity measurements in water, both equations led to equal results, as $\beta > 0.99$ was obtained for all samples. Table 2 shows the results acquired using equation 10. The difference between the diffusion coefficients in the gel phase and those obtained in water increases with increasing dextran molecular size. For dextran 10 kDa, $D/D_0 \sim 0.87$, meaning that there are not many pores in the gel structure with a pore size comparable to the size of this dextran fraction, therefore, its diffusivity is not noticeably affected by the network. However, for a larger molecule such as dextran 500 kDa, $D/D_0 \sim 0.44$, indicating that its diffusivity is significantly restricted by the fibril network.

The echo amplitude shows an exponential decay as a function of G^2 for smaller dextrans, but, a deviation from equation 10 (or 11) is observed for larger dextrans diffusing in the gel net-

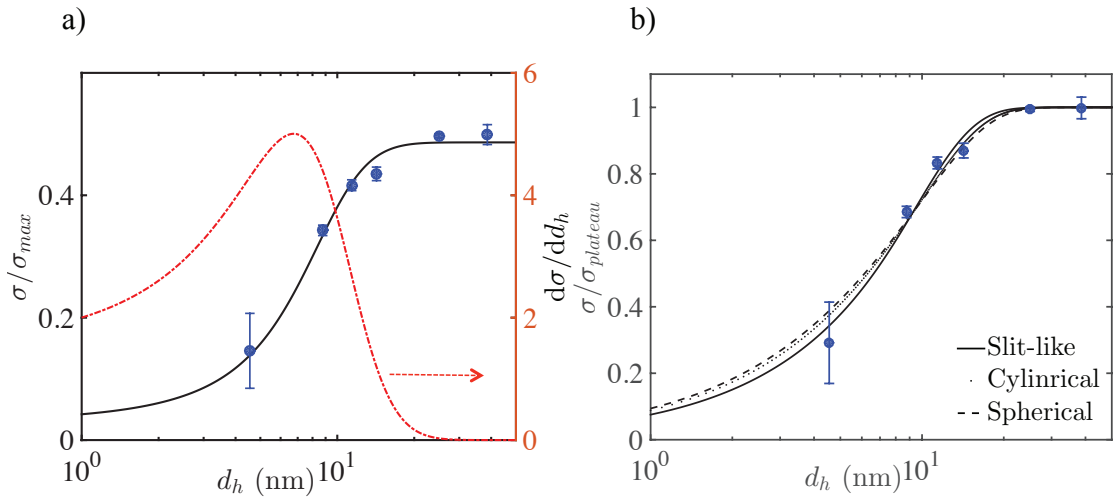

Fig. 4 σ values vs. hydrodynamic diameter d_h for the 0.7% CNF hydrogel cross-linked with DAO. a) Solid line is a fit to equation 2. Dashed line is the corresponding pore size distribution. b) The lines are fits to equation 7 with $K(R_h, r)$ for the three different pore geometries, using equations 3 - 5.

Table 2 Diffusion coefficients in CNF hydrogels, D (m^2 s^{-1}), obtained fitting equation 10 to the experimental data with the goodness of fit R^2_D, the D/D_0 ratios, and the D_g (m^2 s^{-1}) values obtained using the proposed bimodal equation 15 with the goodness of fit $R^2_{D_g}$, for all dextran fractions (kDa)

M_w	$D \times 10^{11}$	R^2_D	D/D_0	$D_g \times 10^{11}$	$R^2_{D_g}$
10	9.2	0.99	0.87	1.6	0.99
40	4.0	0.99	0.73	1.5	0.99
70	2.8	0.99	0.66	1.2	0.99
110	2.1	0.98	0.63	1.1	0.99
500	0.85	0.97	0.44	0.38	0.99
2000	—	0.80	—	0.04	0.99

work. The deviation is significant for dextran 2000 kDa, as shown in figure 5. Wallace et. al. (2013) reported the same for dextrans > 500 kDa diffusing in naphthalene diphenylalanin (2FF) hydrogels. They attributed it to the trapping of large dextran molecules in the gel network.[29] Due to the large deviation from equation 10, we do not report a diffusion coefficient for dextran 2000 kDa inside the gel.

An average mesh size was estimated fitting the diffusion quotients D/D_0 of dextrans 10-500 kDa, to equations 8 and 9. The fibril radius R_f was considered ~ 2 nm. As shown in figure 6, equation 8 fits the diffusivity results better than equation 9 does. An average mesh size $\xi \sim 15$ nm, with $\delta = 0.999$, and an average radius of openings in the fibril network $R_p \sim 10$ nm (pore diameter ~ 20 nm), are obtained in this system for the whole network. However, the wall effect is not considered in developing equations 8 and 9. In addition, the measured diffusion coefficients are not precise for large dextrans, due to the deviation of the exponential equation 10 from the experimental data points; therefore, pore size estimation based on the diffusion quotients may not not be precise for this system.

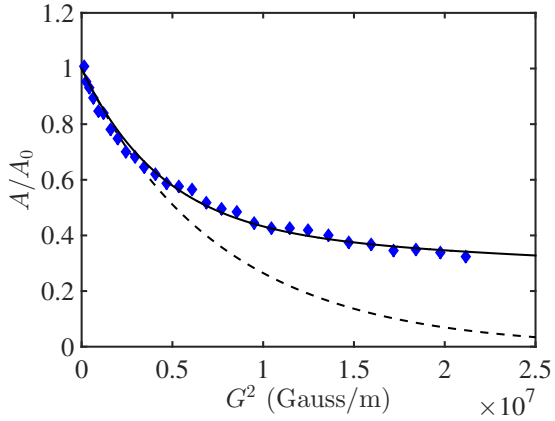

Fig. 5 Normalized echo amplitude vs. G^2, for dextran 2000 kDa in cross-linked 0.7% CNF hydrogel prepared with DAO. $\delta = 0.005$ s, $\Delta = 1.0055$ s. The dashed line is a fit to equation 10, and the solid line is a fit to the proposed bimodal equation 15.

Since our mesh size analysis with solute exclusion method suggests the presence of a group of large openings that even dextran 2000 kDa has access to, we believe that the same should apply to self-diffusion interpretations. Assuming that there are pores large enough not to restrict the diffusivity of the dextran molecules, in which, the probes experience diffusing in the water only, we propose a biexponential model for the echo amplitude decay, as

$$\frac{A(2\tau)}{A_0} = C_g \exp[-bD_g] + (1 - C_g)\exp[-bD_0], \qquad (15)$$

where D_0 is the diffusion coefficient in water, D_g is the diffusion coefficient induced by the gel structure, in the pores that are small enough to affect the diffusivity of the probes, C_g is the fraction of probe molecules that experience the network restrictions, and

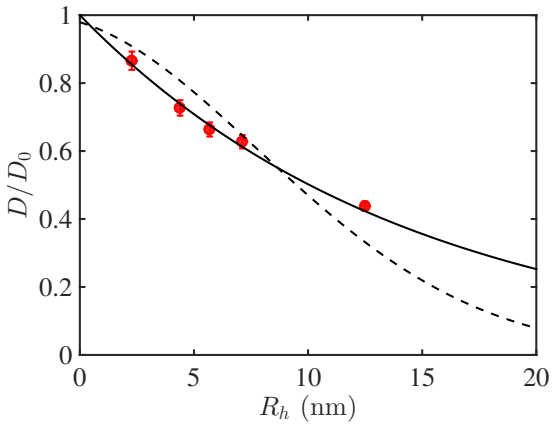

Fig. 6 Diffusion quotients vs. R_h. Solid line is a fit to equation 8, and the dashed line is a fit to equation 9.

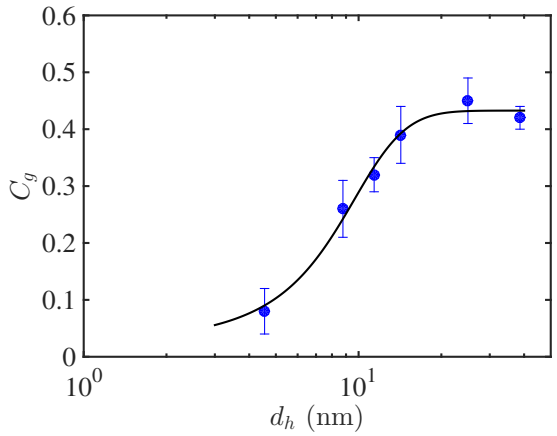

Fig. 7 C_g values obtained using equation 15, vs. d_h. The line is to guide the eye.

$b = (\gamma\delta G)^2(\Delta - \delta/3)$. The PFG-NMR intensity data were fitted to equation 15, using the D_0 values shown in table 1, and D_g, C_g, and A_0 as free parameters. The proposed equation fits the intensity data for all dextrans, including dextran 2000 kDa, very well, as shown in figure 5. The D_g values, shown in table 2, are substantially smaller than the D values, for all dextrans. The D_g/D_0 ratios, however, cannot be used to estimate an average mesh size in the compact region of the hydrogel, using equations 8 or 9. Because the pores, in which the macromolecules experience the network restrictions, are not the same for all dextran fractions.

Variation of C_g as a function of dextran size may give an estimation of the mesh size. As shown in figure 7, C_g increases with increasing d_h, meaning that the number of dextran molecules that experience the network restrictions is larger when the molecular size is larger. The graph reaches a plateau at $d_h \sim 20$ nm. Also $C_g \leq 0.45$, even for the largest dextran fractions, indicating that more than half of the molecules that diffuse into the hydrogel do not experience significant restrictions arising from the fibril network. This confirms our hypothesis on the presence of large openings that do not affect the diffusivity of any of the dextran fractions. Because in NMR experiments, the CNF hydrogels are not exposed to any solution phase, and thus the measurements are not affected by any water swelling or collapsing due to the osmotic forces. This emphasizes the value of solute exclusion results, since the presence of large pores in the fibril network, and the biexponential decay of the echo amplitude with translational diffusion would have not been clear without size exclusion measurements.

We cannot compare our results to the experimental data reported by Masruchin et. al. (2015)[17] for CNF hydrogels prepared with cation cross-linking, because the CNF consistency, the fibril dimensions, and the cross-linking agents are not similar in the two systems. Their SEM images of the freeze-dried aerogels, cross-linked by Al^{3+} or Ca^{2+}, show some large pores with hundreds of nanometers in diameter, and the rest of the pores seem to be around 100 nm, based on the scale bars on the images. The exact CNF consistency is not mentioned. However, they report the pore radius of 2-3 nm for the same aerogels, measured with the BJH method. The significant difference between the output of the two SEM and BJH methods is not explained by the authors.

4.4 Comparison with the theory

In a three-dimensional network of rodlike particles, the average mesh size, representing the spacing between the rods, scales with $\phi^{-0.5}$ as[49,50]

$$\xi = R_f(\frac{\pi}{\phi})^{0.5}, \tag{16}$$

where ϕ is the volume fraction, and R_f is the average radius of the rods. The average mesh size is also estimated in the literature as $\xi = (Ln)^{-0.5}$, where n is the number density, and L is the length of the rods.[51,52] Assuming cylindrical rods, and considering the number density as the ratio of the volume fraction to the volume of an individual rod, this expression leads to equation 16. In our system with $R_f \sim 2$ nm, and $\phi \sim \phi_m/s \sim 0.0047$, where $\phi_m \sim 0.7\%$ is the mass fraction, and $s \approx 1.5$ is the specific gravity of cellulose, equation 16 estimates a mesh size of $\xi \sim 52$ nm for the whole fibril network. From our experimental measurements we know that our cross-linked CNF hydrogel does not have a uniform network structure, but it consists of a number of large openings, containing half of the total amount of water, and more compact regions with smaller mesh units. We can therefore assume that the local volume fraction in the compact parts is twice as large as the bulk volume fraction of the hydrogel. The average mesh size in these regions will then be $\xi \sim 36$ nm with equation 16. This value is not far from our experimental estimation of the mesh size in the compact parts of the hydrogel, obtained with the simple-geometry pore models. The prediction of the spherical pore model in solute exclusion measurements, pore diameter ~ 35 nm, is in very good agreement with the theoretical value. This is not a confirmation of spherical pores in this fibril network, but, it seems that assuming spherical pores is more reasonable than slit-like or cylindrical pores, in this system. Nonetheless, it is obvious that the wall effect and the restrictions on the mobility of the probe molecules in the depletion layer must be taken into account when analysing any solute partitioning or solute self-diffusivity data in porous media.

5 Concluding remarks

Chemically cross-linked CNF hydrogels prepared using diamines are extremely heterogeneous. There is a group of large pores in the hydrogel network, accessible to all dextran molecules, in which, the diffusivity of the molecules is not significantly restricted by the fibril network. The accessibility to the rest of the pores in the dense regions of the network structure is limited, decreasing with increasing the molecular size of the dextrans. The decay of the NMR echo intensity due to translational diffusion in the gel network is biexponential and not single exponential. Depletion layers noticeably affect solute partitioning and self-diffusivity of probe molecules in the gel network.

Acknowledgements

NSERC Innovative Green Wood Fibre Products Network is acknowledged for financial support. We thank Forest Products Laboratory (Madison, WI, USA) for providing the CNF sample, Dr. Tara Sprules for assistance with NMR experiments, and Dr. David Liu for assistance with TEM.

References

1 A. Isogai, T. Saito and H. Fukuzumi, *Nanoscale*, 2011, **3**, 71–85, doi: 10.1039/c0nr00583e.

2 F. W. Herrick, R. L. Casebier, J. K. Hamilton and K. R. Sandberg, *J. Appl. Polym. Sci., Appl. Polym. Symp.*, 1983, **37**, 797–813.

3 A. Lopez-Rubio, J. Lagaron, M. Ankerfors, T. Lindstrom, D. Nordqvist and A. Mattozzi, *Carbohydr. Polym.*, 2007, **68**, 718–727, doi: 10.1016/j.carbpol.2006.08.008.

4 K. L. Spence, R. A. Venditti, O. J. Rojas, Y. Habibi and J. J. Pawlak, *Cellulose*, 2010, **17**, 835–848, doi: 10.1007/s10570–010–9424–8.

5 M. Jorfi and J. Foster, *J. Appl. Polym. Sci.*, 2015, 41719: 1–19 doi: 10.1002/APP.41719.

6 J. Zhao, C. Lu, X. He, X. Zhang, W. Zhang and X. Zhang, *ACS Appl. Mater. Interfaces*, 2015, **7**, 2607–2615.

7 N. Lin and A. Dufresne, *Eur. Poly. J.*, 2014, **59**, 302–325.

8 H. Valo, S. Arola, P. Laaksonen, T. M., L. Peltonen and M. Linder, *Eur. J. Pharm. Sci.*, 2013, **50**, 69–77.

9 M. Paakko, M. Ankerfors, H. Kosonen, A. Nykanen, S. Ahola, M. O. Sterberg, J. Ruokolainen, J. Laine, P. T. Larsson, O. Ikkala and T. Lindstrom, *Biomacromolecules*, 2007, **8**, 1934–1941.

10 M. Henriksson, G. Henriksson, A. Berglund and T. Lindström, *Eur. Poly.*, 2007, **43**, 3434–3441.

11 L. Wågberg, G. Decher, M. Norgren, T. Lindström, M. Ankerfors and K. Axnäs, *Langmuir*, 2008, **24**, 784–795.

12 A. Pei, N. Butchosa, L. A. Berglund and Q. Zhou, *Soft Matter*, 2013, **9**, 2047–2055.

13 L. Jowkarderis and T. van de Ven, *Cellulose*, 2014, **21**, 2511–2517, doi: 10.1007/s10570–014–0292–5.

14 L. Jowkarderis and T. van de Ven, *Carbohydr. Polym.*, 2015, **123**, 416–423.

15 N. Lin and A. Dufresne, *Biomacromolecules*, 2013, **14**, 871–80.

16 X. Zhang, J. Huang, P. Chang, J. Li, Y. Chen and D. Wang, *Polymer*, 2010, **51**, 4398–4407.

17 N. Masruchin, B. Park, V. Causin and I. Um, *Cellulose*, 2015, doi: 10.1007/s10570–015–0624–0.

18 Z. Wang and R. K. Marcus, *J. Chromatography*, 2014, **1351**, 82–89.

19 S. M. Russell and G. Carta, *Ind. Eng. Chem. Res.*, 2005, **44**, 8213–8217.

20 M. Ousalem, X. X. Zhu and J. Hradil, *J. Chromatography*, 2000, **903**, 13–19.

21 D. H. Walther, G. H. Sin, H. W. Blanch and J. M. Prausnitz, *Polymer Gels and Networks*, 1995, **3**, 29–45.

22 L. J. Aggerbrandt and O. Samuelson, *J. Appl. Polym. Sci.*, 1964, **8**, 2801–2812.

23 J. K. Lin, M. R. Ladisch, J. A. Patterson and C. H. Noller, *Biotechnology and Bioengineering*, 1987, **29**, 976–981.

24 J. C. Day, B. Alince and A. A. Robertson, *Cellul. Chem. Technol.*, 1979, **13**, 317.

25 B. H. Van Dyke, *Ph.D. thesis*, Massachusetts Institute of Technology, 1972.

26 J. Stone and A. Scallan, *Cellulose Chem. Technol.*, 1968, **2**, 343–358.

27 G. Guillot, L. Leger and F. Rondelez, *Macromolecules*, 1985, **18**, 2531–2537.

28 D. Langevin and F. Rondelez, *Polymer*, 1978, **19**, 875–882, doi:10.1016/0032–3861(78)90191–X.

29 M. Wallace, D. Adams and J. Iggo, *Soft Matter*, 2013, **9**, 5483–5491.

30 S. Matsukawa and I. Ando, *Macromolecules*, 1997, **30**, 8310–8313.

31 A. Rolleri, F. Burgos, C. Bravo-Linares, E. Vásquez and F. Droppelmann, *Wood Sci. Technol.*, 2014, **48**, 787–795.

32 E. F. Casassa, *Polym. Lett.*, 1967, **5**, 773–778.

33 Y. Yao and A. M. Lenhoff, *J. Chromatography A*, 2004, **1037**, 273–282.

34 M. Quesada-Pérez, I. Adroher-Benitez and J. A. Maroto-Centeno, *J. Chem. Phys.*, 2014, **140**, 204910–1:7.

35 *The Nanoscience and Technology of Renewable Biomaterials*, ed. L. A. Lucia and O. J. Rojas, Blackwell Publishing Ltd, 2009.

36 T. Lindström and G. Carlsson, *Sven. Papperstidn*, 1982, **85**, 14–20.

37 J. Grignon and A. M. Scallan, *J. Appl. Polym. Sci.*, 1980, **25**, 2829.

38 A. A. Gorbunov, L. Y. Solovyova and V. A. Pasechnik, *J. Chromatography*, 1988, **448**, 307–332.

39 R. I. Cukier, *Macromolecules*, 1984, **17**, 252–255.

40 S. Matsukawa, D. Sagae and A. Mogi, *Progr Colloid Polym Sci*, 2009, **136**, 171–176, doi: 10.1007/2882–2009–24.

41 B. Amsden, *Macromolecules*, 1999, **32**, 874–879, doi: 10.1021/ma980922a.

42 A. Altieri, D. Hinton and R. Byrd, *J. Am. Chem. Soc.*, 1995, **117**, 7566–7561.

43 B. Håkansson, M. Nydén and O. Söderman, *Colloid Polym. Sci.*, 2000, **278**, 399:405.

44 K. Braeckmans, L. Peeters, N. Sanders, S. De Smedt and J. Demeester, *Biophys. J.*, 2003, **85**, 2240–2252.

45 M. Kunishima, C. Kawachi, K. Hioki, K. Terao and S. Tani, *Tetrahedron*, 2001, **57**, 1551–1558.

46 F. C. MacKintosh, J. Käs and P. A. Janmey, *Phys. Rev. Lett.*, 1995, **75**, 4425–4428.

47 L. Pescosolido, L. Feruglio, R. Farra, S. Fiorentino, I. Colombo, T. Coviello, P. Matricardi, W. E. Hennink, T. Vermondend and M. Grassi, *Soft Matter*, 2012, **8**, 7708–7715.

48 A. G. Byju, A. Kulkarni and N. Gundiah, 13th International Conference on Fracture, ICF, 2013, pp. 4406–4415.

49 *Structure and Dynamics of Strongly Interacting Colloids and Supramolecular Aggregates in Solution*, ed. S. Chen, J. Huang and P. Tartaglia, Springer, Netherlands, pp 504-505, 2012.

50 M. R. King and N. A. Mody, *Numerical and Statistical Methods for Bioengineering: Applications in MATLAB*, Cambridge University Press, pp 199-210, 2010.

51 M. Das and F. C. MacKintosh, *Phys. Rev. Lett.*, 2010, **105**, 138102:1–4, doi: 10.1103/PhysRevLett.105.138102.

52 K. Salamon, D. Aumiler, G. Pabst and T. Vuletič, *Macromolecules*, 2013, **46**, 1107–1118.

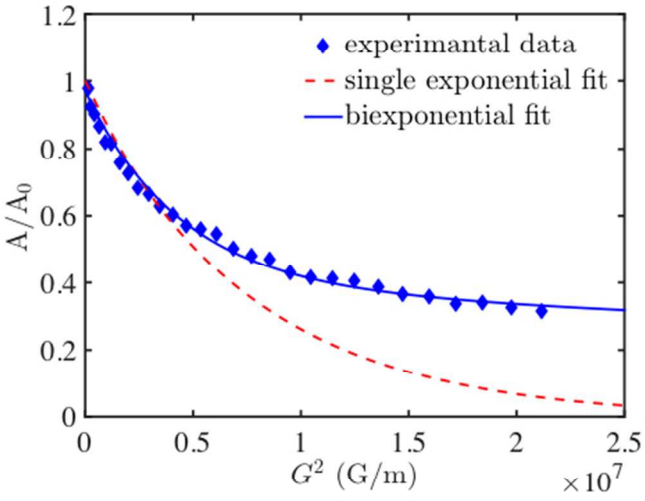

The decay of the NMR echo intensity due to translational diffusion in the heterogeneous gel network is biexponential.

The decay of the NMR echo intensity due to translational diffusion in the heterogeneous gel network is biexponential.

254x190mm (72 x 72 DPI)